ACS APPLIED ELECTRONIC MATERIALS

pubs.acs.org/acsaelm Article

Small Electron Polaron in Carbon-Doped Cubic Boron Nitride

Sharmila N. Shirodkar, Cyrille Armel Sayou Ngomsi, and Pratibha Dev*

Cite This: https://doi.org/10.1021/acsaelm.2c01743 Read Online

ACCESS | Metrics & More | Article Recommendations | Supporting Information

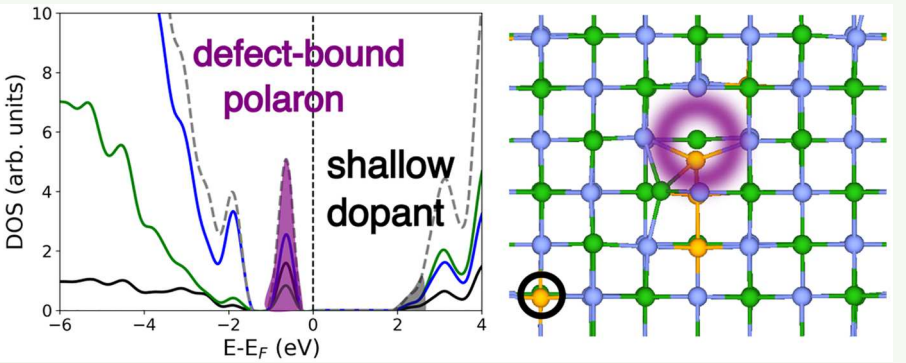

ABSTRACT: Controllable and reliable doping of cubic boron nitride (cBN) is a critical challenge in its widespread application in power electronics. Recently, progress was made in this regard when an experiment reported successful n-doping of cBN with carbon, reaching carbon concentrations as high as 5%, which is beyond the thermodynamic solubility limit. However, the nature of carbon-based defects introduced within the cBN matrix remains unknown thus far. Here, we explore the electronic structure of carbon-doped cBN under nitrogen-rich conditions, which are conducive to the formation of donor-type defects (such as carbon substituents replacing boron), and predict several possible arrangements of carbon in clusters at experimentally relevant concentrations of 1.5−7.8%. Our theoretical calculations show that carbon dopants prefer to aggregate into small clusters with local ordering rather than distributing randomly in the bulk. Along with defects that result in easily ionizable defect states, we also report a distribution of carbon dopants, where the structure exhibits a defect-bound small electron polaron. The polaron can be identified via a split-off localized dopant band near the valence band edge. These findings not only shed light on identities of possible carbon-based defects but also predict additional carriers—defect-bound small polarons.

KEYWORDS: *cBN, n-doping, carbon doping, defect-bound polarons, small polarons*

1. INTRODUCTION

Cubic boron nitride (cBN) is known for its stability and an ultrawide band gap of 6.1 eV,[1] qualities that enable its use in applications demanding extreme pressures and temperatures and high power.[2−5] Notwithstanding numerous reports of successful n-doping[4,6,7] and p-doping[8−10] of cBN since the late 1980s, doping it controllably and reliably with the precision required for optoelectronics applications had proved to be difficult over the decades. Recent advances in experimental techniques, in particular pulsed laser deposition, has allowed Haque et al.[11] to controllably n-dope cBN using up to 5% carbon (C), a concentration about 100 times higher than the thermodynamic solubility limit of 0.08%. These high doping levels open up new possibilities for the use of cBN in electronic and optical high-power applications.

To date, however, the identities of the C-based defects introduced in the experiment by Haque et al.[11] have remained unknown. It is also not clear if the impurity atoms in C-doped cBN result in any of the doping-bottleneck issues that were recently discussed by Joshi et al.[12] For example, it was shown[12] that carbon is an amphoteric impurity, which can replace boron (as an n-dopant) as well as nitrogen (as a p-dopant). Carbon impurity as C_B was shown to produce a shallow donor state, while as C_N it produces deep acceptor states. Further, these substituents were also shown to compensate for each other, without introducing ionizable states. It should also be pointed out that recent works[12−14] indicate that the lattice distortions upon defect formation/doping can lead to the formation of polaron states in cBN. Polaron states are charge trapping levels that result from lattice distortions induced by doping. Notably, Joshi et al.[12] report a polaronic state in cBN codoped with both silicon and oxygen that traps electrons to the defect site. This is not surprising as defect-bound small

Received: December 19, 2022
Accepted: February 19, 2023

polarons[15,16] have been reported in other wide band gap semiconductors, such as TiO_2[17] and ZnO[18]. As there are a number of possible outcomes, including formation of trap states/polarons upon C-doping, which have not been studied to date, it is important to consider different possible distributions of the C impurity in cBN at the experimentally relevant concentrations.

In our first-principles density functional theoretical (DFT) based work, we study (a) how carbon dopants distribute in the cBN lattice under N-rich conditions, since these conditions are conducive to the formation of donor-type defects (such as the carbon substitutional, C_B), and (b) different configurations that can lead to self-trapped charge states/polaron states. This is achieved by exploring in detail the symmetry inequivalent ways in which carbon dopants can be distributed in the cBN matrix at high doping concentrations (1.5−7.8%) and their lowest energy configuration at each particular concentration. We show that C-doping can result in a combination of defects that induce easily ionizable defect states as well as carbon distributions that result in the formation of trap states/defect-bound polarons.[19] Since in experiments both types of carbon distributions will be present, one expects to see the signatures of these doping outcomes in the electrical transport properties of the doped cBN. Note that even if small polarons are charge traps, they still give rise to nonzero electrical conductivity via trapped carrier hopping between sites by thermally induced lattice distortions.[20,21] In fact, Haque et al.[11] found a sharp increase in resistivity below 35 K, which they attribute to the presence of partial ionization and freeze-out regions. Our results indicate that, at low temperatures, the experimentally observed charge transport might have contributions from both partially ionized shallow states and defect-bound polaron hopping. However, since these defect-bound polarons are tightly bound to the carbon clusters, we expect them to conduct via impurity hopping or defect migration and not via thermally induced lattice distortions. We explore the energy barriers for the polarons to hop via lattice deformations and draw inferences to explain the experimentally observed behavior of resistivity with temperature.

2. COMPUTATIONAL METHODS

Spin-polarized density functional theoretical (DFT) calculations were carried out with the Quantum Espresso package.[22] We used a plane wave basis set with a mesh cutoff of 55 Ry and a charge density cutoff of 400 Ry. The electron−ion interactions were modeled with ultrasoft pseudopotentials,[23] and the exchange−correlation energy of the electrons was treated within the generalized gradient approximation (GGA) functional of Perdew−Burke−Ernzerhof (PBE) .[24] The structures were relaxed until the Hellmann−Feynman forces on each atom were smaller in magnitude than 0.7 meV/Å, and the energy difference between relaxation steps was converged below 0.1 meV. The Brillouin zone (BZ) integrations were carried out over an 8 × 8 × 8 Monkhorst−Pack *k*-point mesh for the conventional cubic unit cell of cBN with eight atoms. We modeled the C dopants in a 2 × 2 × 2 cBN supercell with 64 atoms, for which we used a 4 × 4 × 4 Monkhorst−Pack *k*-point mesh. The calculations using a 3 × 3 × 3 cBN supercell are discussed in the Supporting Information.

Different symmetry inequivalent configurations at a given concentration of doping were generated with the Site Occupancy Disorder (SOD) package.[25] This allowed us to explore varied doping configurations and to predict the ground state structures that would most probably persist in experimental samples and also exhibit high charge carrier concentrations. In addition, we also generated random alloy configurations that mimic totally disordered alloys using the special quasi-random structure (SQS) method[26,27] as implemented in the "mcsqs" utility of the Alloy Theoretic Automated Toolkit package.[28]

The formation energy ($E_{formation}$) of the doped structures was calculated using the following expression:

$$E_{formation} = E_{C-BN} - (n_C\mu_C + n_B\mu_B + n_N\mu_N) \quad (1)$$

where n_C, n_B, and n_N are the number of C dopants, B atoms, and N atoms in the doped supercell, respectively; E_{C-BN} is the total energy of the doped supercell; and μ_C, μ_B, and μ_N are the chemical potentials of C, B, and N, respectively. The chemical potential for C (μ_C) was calculated with respect to an isolated atom and C in graphene. The chemical potentials, μ_B and μ_N, in the N-rich conditions obtained using N_2 and cBN as reference and under B-rich conditions obtained using αB and cBN as reference, were calculated as follows:

$$\mu_N = E(N_2)/2; \qquad \mu_B = E(BN) - \mu_N \quad (2)$$

under N-rich conditions and

$$\mu_B = E(\alpha B)/12; \qquad \mu_N = E(BN) - \mu_B \quad (3)$$

under B-rich conditions. Here, E(BN), $E(\alpha$B), and $E(N_2)$ are the energies of cBN per formula unit, α-boron (with 12 atoms/cell), and N_2, respectively.

3. RESULTS AND DISCUSSION

3.1. Dopant Clustering and Formation Energy. We first explore the possible doping configurations of carbon dopants in a 2 × 2 × 2 supercell of 64 atoms at concentrations of 1.5−7.8% (i.e., 1−5 C/cell). We use the SOD[25] package to determine the symmetry inequivalent configurations of carbon doping in the supercell and estimate their formation energies. Details of these calculations can be found in the Supporting Information. Here, we use $\mathcal{N}_N$ and $\mathcal{N}_B$ to denote the number of carbons occupying the nitrogen (C_N) or boron (C_B) sites, and $\mathcal{N}_B C_B \mathcal{N}_N C_N$ to denote the configurations at a particular doping concentration. We note that, for a given concentration of carbon dopants (number of carbon dopants per supercell), there are several ways to divide the carbon at nitrogen and boron sites. Since the experimental samples[11] are n-doped, we only consider configurations with $\mathcal{N}_B \geq \mathcal{N}_N$ namely, C_B (1.5% doping) (and C_N for reference), $2C_B$ (3%), C_BC_N (3%), $2C_B1C_N$ (4.7%), $2C_B2C_N$ (6.25%), $3C_B1C_N$ (6.25%), $3C_B2C_N$ (7.8%), and $4C_B1C_N$ (7.8%). Also, under N-rich conditions, the formation energies of C_B and C_N substituents were shown to be comparable, with a slight preference for the formation of the former defect than for the latter one.[12] This means that, although tetravalent carbon dopants can occupy both trivalent boron and pentavalent nitrogen sites, there will be a small excess of C_B(s), imparting the sample its n-type behavior. In addition to the symmetry inequivalent configurations, we also generate special quasi-random structures (SQSs)[26,27] for each $\mathcal{N}_B C_B \mathcal{N}_N C_N$ configuration, to explore if the doping results in a random alloy with little/no correlation between the dopants and the atom types on any other lattice site.

Our estimates of the formation energy ($E_{formation}$) confirm that the n-doped ($\mathcal{N}_B \geq \mathcal{N}_N$) configurations are considerably lower in energy under N-rich conditions. The lowest (ground

https://doi.org/10.1021/acsaelm.2c01743
ACS Appl. Electron. Mater. XXXX, XXX, XXX−XXX

Table 1. Formation Energies (in eV) of Ground State $\mathcal{N}_B C_B \mathcal{N}_N C_N$ Configurations under N-Rich and B-Rich Conditions

$\mathcal{N}_B C_B \mathcal{N}_N C_N$	C_B	C_N	$2C_B$	$C_B C_N$	$2C_B 1C_N$	$2C_B 2C_N$	$3C_B 1C_N$	$3C_B 2C_N$	$4C_B 1C_N$
$E_{formation}$ for N-rich (eV)	4.4	4.5	8.8	2.9	6.2	4.9	8.9	8.1	12.0
$E_{formation}$ for B-rich (eV)	6.8	2.1	13.6	2.9	8.6	4.9	13.7	10.5	19.2

state) $E_{formation}$ values for each doping concentration under N-rich and B-rich conditions are given in Table 1. The formation energies for all the other symmetry inequivalent (higher energy) configurations can be found in the Supporting Information. Except for $4C_B1C_N$, which is magnetic (with a moment of $1\mu_B$), none of the other ground state structures exhibit magnetization, although some of the higher energy structures exhibit nonzero magnetization with spin-polarization energies of ≈220 meV and also a total magnetic moment of $1\mu_B$ (mostly concentrated on a carbon atom at a boron site) at all concentrations. These local moments originate from the highly localized nature of defect states, which are themselves derived from the 2s and 2p states of the second row elements of the p-block (carbon and neighboring nitrogens).[29−31] The formation energies at higher doping concentrations given in Table 1 seem prohibitively large. However, we note that the pulse laser deposition technique used to experimentally achieve these doping levels[11] would be able to provide the necessary energy to achieve them. Furthermore, the energies of SQS structures are higher than the ground state energies (see Table S1 and Figure S2). In turn, this confirms the existence of smaller local ordered structures, consisting of specific C arrangements/cluster instead of a totally random disordered alloy.[32]

The preferred carbon doping positions in the ground states of $\mathcal{N}_B C_B \mathcal{N}_N C_N$ systems are shown in Figure 1. Overall, we find

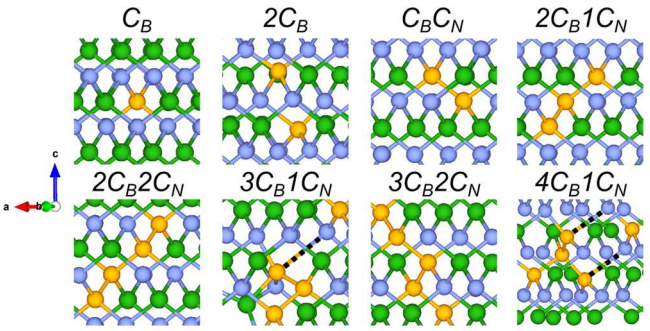

Figure 1. Distribution of carbon atoms in the ground state configurations for $\mathcal{N}_B C_B \mathcal{N}_N C_N$. The carbon atoms are shown as yellow spheres, boron atoms are shown as green spheres, and nitrogen atoms are shown as blue spheres. The broken C−N bonds are highlighted by black dashed lines. Note that the C_N configuration is same as C_B but with the positions of B and N interchanged.

that when we go beyond the isolated case of C_B and C_N, carbons tend to form small clusters, occupying nearest-neighbor and/or next-nearest-neighbor sites, similar to carbon in hexagonal BN.[33] In particular, the carbon atoms in the ground states of C_BC_N, $2C_B1C_N$, $2C_B2C_N$, and $3C_B2C_N$ form continuous chains. In $3C_B1C_N$, the lowest energy structure shows a substantial local distortion that breaks the C−N bond between one of the carbon atoms and the nitrogen atom that links two of the carbons in the cluster. This is highlighted by the black dashed line in Figure 1, indicating the C−N distance of ≈2.38 Å after the bond breaking (cf. C−N distance of ≈1.52 Å in the isolated C_B defect). Also, $4C_B1C_N$ shows distortions similar to $3C_B1C_N$ with the extra carbon substituting the B atom in the tetrahedron instead in a chain. This configuration leads to the breaking of two C−N bonds (with C−N distance of ≈2.22 Å). Since $3C_B1C_N$ and $4C_B1C_N$ ground state configurations show considerable local distortions that break C−N bonds, we hypothesize that these two configurations are the most likely candidate structures with small polarons. Hence, we next explore the electronic structures of these two configurations in detail.

3.2. Electronic Structure: C-Doped cBN. We begin by inspecting the doping concentrations and carrier densities of the ground state structures for all of the $\mathcal{N}_B C_B \mathcal{N}_N C_N$ configurations. For a configuration with $\mathcal{N}_B > \mathcal{N}_N$, one would expect n-doping (since C has one more valence electron than B) with the net charge doped equal to $1e(\mathcal{N}_B - \mathcal{N}_N)$. Hence, C_B, $2C_B1C_N$, and $3C_B2C_N$ correspond to 1 electron/cell doping, whereas $3C_B1C_N$ and $4C_B1C_N$ correspond to 2 and 3 electrons/cell, respectively. To check whether these doping configurations are indeed contributing to the carrier density, we studied their electronic densities of states (DOSs). These DOS plots (and band structures) can be seen in Figure 2 for $3C_B1C_N$ and $4C_B1C_N$ and in Figures S3 and S4 for the rest of the carbon concentrations considered here. We find that C_B and C_N indeed correspond to n- and p-doping of 1 electron/cell and 1 hole/cell, respectively, in agreement with Joshi et al.[12] Similarly, C_BC_N and $2C_B2C_N$ correspond to no net doping, resulting in insulating structures with a wide band gap of ≈4 eV (similar to pure cBN). The ground state of $2C_B$ corresponds to two adjacent carbons separated by a nitrogen atom. In $2C_B$, each C-dopant contributes 1 electron/cell, corresponding to a carrier density of 6×10^{21} cm^{-3}. This is comparable to the carrier density reported for 5% dopant concentration by Haque et al.[11] (see the Supporting Information). Similarly, $2C_B1C_N$ contributes 1 electron/cell, i.e., a free charge carrier concentration of 3×10^{21} cm^{-3}. We also confirmed these values by integrating the charge density from inside the band gap until the Fermi level and the charge density distribution in the lattice space (see Table S4).

As suspected based on the extent of distortion, the ground state structure of $3C_B1C_N$ does exhibit a polaron state (see Figure 2A,B). The state is identified as a dopant localized state below the Fermi level that is split off from the conduction band by ≈3 eV. We find a charge of 2 electrons/cell by integrating the DOS of this localized dopant state, which is in agreement with the expected charge carrier density induced by the configuration. Hence, the $3C_B1C_N$ configuration does not lead to the shallow doping of the cBN matrix. On the other hand, $4C_B1C_N$ is a half-metal with a conducting spin-down channel dopant state and an insulating spin-up dopant state, even if both spin-up and spin-down channels are split off from the conduction band (see Figure 2C,D). Hence, this is a conducting state that contributes to the free charge carrier density and therefore cannot be clearly identified as a polaron. However, the symmetry in the broken bonds (see Figure 1) and "splitting + localization" of the charges to the C and N sites (see Figure S6H,I) does not discount the possibility of a

https://doi.org/10.1021/acsaelm.2c01743
ACS Appl. Electron. Mater. XXXX, XXX, XXX−XXX

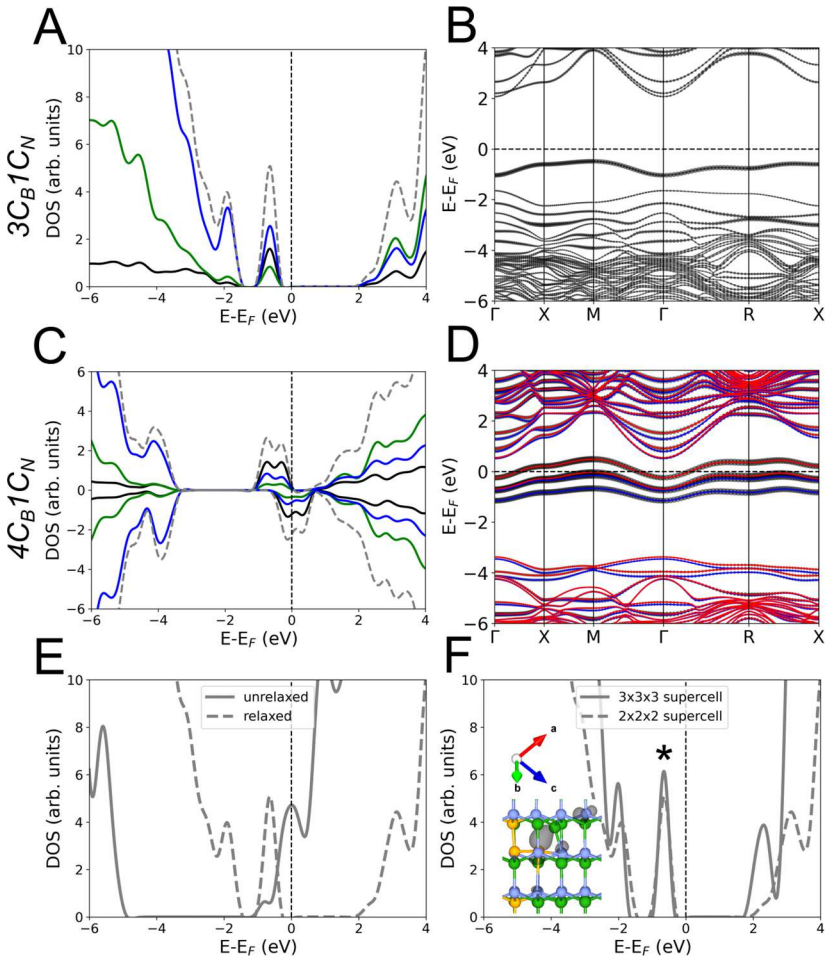

Figure 2. Electronic density of states (DOS) and band structures for ground state configurations. The DOSs for (A) $3C_B1C_N$ and (C) $4C_B1C_N$ projected onto the chemical species are shown in blue solid curves for nitrogen, green solid curves for boron, and black solid curves for carbon. The total DOSs are shown in gray dashed lines. The positive and negative DOSs in (C) are for the spin-up and spin-down channels, respectively. The fat band plots for (B) $3C_B1C_N$ and (D) $4C_B1C_N$ showing contributions from the carbon atoms to the band structures are given as black circles. The blue and red curves in (D) represent the spin-up and spin-down channels, respectively. Changes in DOS of $3C_B1C_N$ (E) for unrelaxed (solid gray lines) and relaxed (dashed gray lines) structures and (F) in $3 \times 3 \times 3$ supercell (solid gray lines) and $2 \times 2 \times 2$ supercell (dashed gray lines). The inset in (F) shows the integrated charge density distribution (black) of the polaron state (denoted by $*$). The carbon atoms are shown as yellow spheres, boron atoms are shown as green spheres, and nitrogen atoms are shown as blue spheres. Panel F confirms that the stress due to the fixed lattice constant (supercell size) and the dopant density are not responsible for the state being nonconducting.

bipolaron,[34] and remains a topic for future work. Furthermore, we note that cBN is piezoelectric and the strain in $4C_B1C_N$ due to bond breaking should give rise to local electric dipole moments around the carbon clusters. Since the ground state of this configuration is also magnetic, a coupling between the electric and magnetic degrees of freedom will give rise to magnetoelectric effects, and hence these carbon clusters could be explored for applications in memory devices.

To confirm that the polaron state in $3C_B1C_N$ arises from the distortion of the cBN lattice on doping and not by the supercell size, we carried out calculations on its undistorted ground state structures. The total DOSs in nondistorted (unrelaxed) and distorted (relaxed) ground state structures of $3C_B1C_N$ are compared in Figure 2E. We find that the electronic structure undergoes a drastic change as the lattice relaxes and the system goes from an undistorted (unrelaxed) conducting state to a distorted (relaxed) semiconducting state. This analysis also allows us to calculate the polaron formation energy, E_{Polaron},[35,36] which is defined as the difference in total energies of distorted structure with a localized charge ($E^{\text{loc}}_{\text{dist}}$) and the undistorted structure ($E^{\text{unloc}}_{\text{undist}}$), which displays a delocalized excess charge from C-doping. We find that $E_{\text{Polaron}} = E^{\text{loc}}_{\text{dist}} - E^{\text{deloc}}_{\text{undist}} = -2.55$ eV. It represents a net lowering of energy resulting from a competition between the energy cost of distorting the cBN lattice and the energy gained by the localization of the electron in the distorted structure. We estimate $E_{\text{Polaron}} = -3.23$ eV for the $4C_B1C_N$ ground state. Furthermore, to dismiss the interaction between the periodic images of the carbon clusters as being the factor for the polaronic state, we calculated the DOS for the same clustering of carbon atoms (see Figure 1) in a $3 \times 3 \times 3$ supercell. Figure 2F compares the DOS plots for $2 \times 2 \times 2$ and $3 \times 3 \times 3$ supercells. It shows that we indeed have a defect-bound polaronic state.[19,37] We find no change in the position of the dopant state with respect to the Fermi level, and a plot of its charge density shows that it is also localized to the carbon cluster (see Figure 2F, inset). Hence, we confirm the presence of small polarons in carbon-doped cBN. Lastly, since screened hybrid functionals estimate the band gap and electronic structure more accurately than the PBE functional, we

https://doi.org/10.1021/acsaelm.2c01743
ACS Appl. Electron. Mater. XXXX, XXX, XXX−XXX

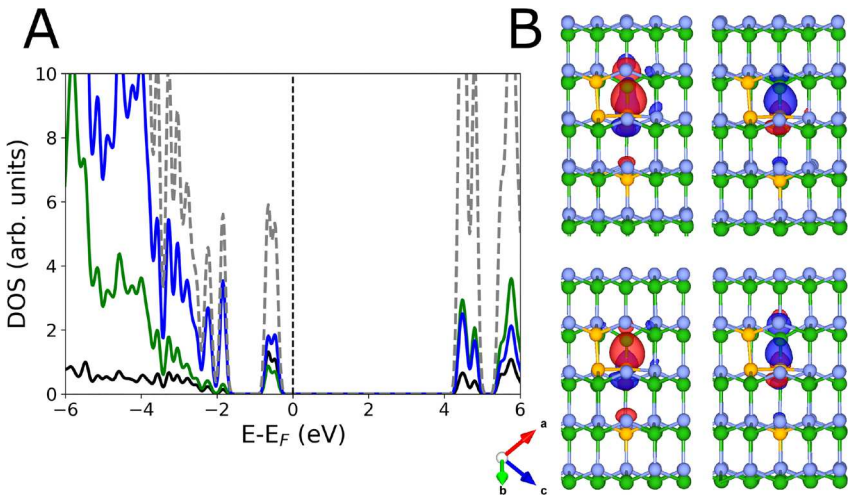

Figure 3. Electronic density of states (DOS) for the ground state configuration of $3C_B1C_N$ using the HSE06 functional. (A) DOS projected onto the chemical species: blue solid curves for nitrogen, green solid curves for boron, and black solid curves for carbon. The total DOSs are shown in gray dashed lines. (B) Real part of the charge density distribution (red/blue) of the wave functions constituting the polaron state below the Fermi level. The four plots belong to the same band but different k points. The red and blue colors distinguish the opposite phases of the wave functions. The carbon atoms are shown as yellow spheres, boron atoms are shown as green spheres, and nitrogen atoms are shown as blue spheres.

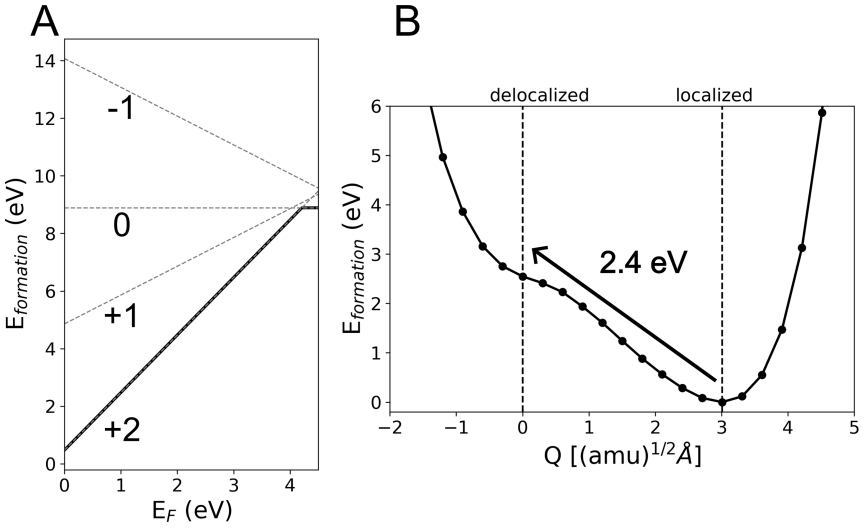

Figure 4. Formation energy and activation barriers for the $3C_B1C_N$ polaronic state. (A) Formation energy in different charge states (−1, 0, +1, +2) with respect to the Fermi energy referenced to zero at VBM in pristine cBN under nitrogen-rich conditions. Gray dashed lines indicate the formation energies of different charged states, and the black solid line is the minimum formation energy curve for every value of the Fermi energy. (B) Variation in energy of the polaronic state with deformation going from the undistorted [$Q = 0$ (amu)$^{1/2}$ Å] to the distorted [$Q = 3$ (amu)$^{1/2}$ Å] structure in the neutral charge state.

recalculated the electronic structure of the $3C_B1C_N$ ground state using HSE06.[38] The Supporting Information provides the details for the HSE06 calculations. As expected, we find that the band gap increases from 4 eV with PBE to ≈6 eV with HSE06 (see Figure 3). The DOS plot in Figure 3 shows that our HSE06 results are in qualitative agreement with those obtained using PBE (see Figure 2A). Within HSE06, the structure is again predicted to be insulating, with a polaron (defect) state below the Fermi level. The charges in the polaron state are localized near the carbon dopants (see Figure 3B). Since our PBE results are robust, and the electronic structure does not change qualitatively, we do not repeat the HSE06 calculations for the rest of the structures presented in this work.

Similar comparisons of DOSs with distortion and supercell size for $4C_B1C_N$ can be found in Figure S5. We note that our calculations are used to confirm polaron formation in the carbon-doped cBN. However, we do not claim a particular configuration, such as $3C_B1C_N$, to be the most stable or the only polaronic state possible. There might be many other such configurations of small carbon clusters that result in polaron formation, with the polaron formation energy even lower than that for $3C_B1C_N$, which are more likely to occur. It should be also noted that other higher energy structures of $2C_B1C_N$ and $3C_B2C_N$ which are 0.53 and 0.55 eV, respectively, higher in energy as compared to their ground state configurations, also exhibit polaronic states. These states are partially localized at the nitrogen atoms surrounding the dopant carbon atoms (see Figure S6). The energies of these structures are considerably high and cannot form at room temperatures. However, we can expect them to be stabilized under nonequilibrium conditions

https://doi.org/10.1021/acsaelm.2c01743
ACS Appl. Electron. Mater. XXXX, XXX, XXX−XXX

and possibly frozen into the structure during pulsed laser deposition.

4. CHARGE STATES AND ACTIVATION BARRIERS

The temperature dependent resistivity measurements by Haque et al.[11] show two regimes in carbon-doped cBN: (i) a high temperature regime (≥35 K) with higher activation energies and resistivity decreasing with temperature and (ii) a low temperature regime (<35 K) where the resistivity increases with a decrease in temperature with a lower activation energy. The authors attribute these two regimes to "partial ionization region or the freeze-out regions that can be reached at different temperatures"[11] but do not elaborate on the types of carriers that are responsible for such behavior. In order to evaluate whether different polaronic defects contribute to the conduction in the experimental samples, we explore the charge state transition levels of these defects and predict their stability in experimental samples. Focusing on the $3C_B1C_N$ polaronic defect, we also estimate the thermal activation barrier of the neutral polaronic state and compare it with the experimental values given by Haque et al.[11] Refer to the Supporting Information for the charge transition levels of the other polaronic defect, $4C_B1C_N$.

From Figure 4A) we find that the $3C_B1C_N$ defect is a double donor, as expected, and exists in the +2 charge state for most of the doping regimes, whereas the neutral state stabilizes in the highly n-doped region. The (+2/0) transition state is at ≈4.2 eV above the valence band maximum (VBM), with a donor ionization energy of 4.5 − 4.2 = 0.3 eV (with respect to the conduction band minimum, CBM) for the transition of the defect from the neutral to the +2 charge state. We note that the structural ground state of the +2 charge state is nearly undistorted (cubic) and the neutral ground state structure is distorted with broken C−N bonds (see Figure 1). This is as expected—in the neutral charge state, the lattice distorts owing to the localized nature of the defect states with the excess charges (coming from donor carbons). On the other hand, in the +2 charge state the excess electrons have been removed from the defect, obviating the need for the lattice to distort in response to localized defect states. Since cBN is heavily doped with carbon in the experiment,[11] with defects such as C_B giving rise to efficient n-type doping of the system, it is reasonable to assume that the Fermi level in the doped structures will be closer to the CBM, resulting in the neutral polaronic-type state for $3C_B1C_N$ defect. To check whether temperature variation in the Fermi level (E_F) can lead to the neutral to +2 charge transition, we estimated the position of E_F for an extrinsic semiconductor using the expression for the defect formation energy as a function of temperature (T) as described by Coutinho.[39] Assuming a donor density of 10^{19} cm^{-3}, we get E_F = 0.05 eV (at 50 K), 0.12 eV (at 100 K), 0.25 eV (at 200 K), 0.39 eV (at 300 K), and 0.53 eV (at 500 K) from the CBM (details can be found in the Supporting Information). As the temperature increases, the Fermi level moves from the CBM to below the +2/0 transition level. This results in the transitioning of the $3C_B1C_N$ defect from the localized polaronic bound state to the conducting undistorted structure in the +2 charged state. We note that ionization of $3C_B1C_N$ defect-bound polarons will in turn n-dope the sample and shift the Fermi level toward the CBM. Depending upon the number of ionized $3C_B1C_N$ donors, as well as the concentrations of other shallow defects (as the carbon concentration is increased), the Fermi level could move back to a near-CBM region in the band gap, resulting in a neutral charge state for the defects, such as $3C_B1C_N$, that retrap the charge carriers at the $3C_B1C_N$ clusters. Hence, the system will reach a ionized defect concentration that will curb any further n-doping of the sample. On the basis of our estimate of the charge transition level and the Fermi level as a function of temperature, we hypothesize that the experimental samples at room temperature will have contributions from the $3C_B1C_N$ defect in the +2 charge state due to their free charge carriers, whereas at low temperatures polaron transport will become more dominant (see below).

We also determined whether the neutral $3C_B1C_N$ polaron can conduct via thermal hopping. To do so, we evaluated the potential energy surface along the distortion (denoted by the generalized coordinate Q) that takes the localized/distorted neutral state [Q = 3 (amu)$^{1/2}$ Å] to the delocalized/undistorted state [Q = 0 (amu)$^{1/2}$ Å] for the neutral state (see Figure 4B). The delocalized (undistorted) neutral state has no barrier to self-trap and hence makes a transition to the localized (distorted) Q = 3 (amu)$^{1/2}$ Å neutral state, which traps the carriers. On the other hand, the transition from the localized state to the delocalized state is ≈2.5 eV, which is considerably higher than the activation barriers reported in experiments.[11] It is, therefore, unlikely to take place through this mechanism. However, there are other possible migration pathways (via vacancies or coupling with Fröhlich polarons[40]) that can aid polaron hopping, but their exploration is currently beyond the scope of this work.

5. CONCLUSIONS

We have carried out systematic first-principles calculations to predict distributions of highly doped cBN, with C-dopant concentrations in the range 1.5−7.8%. Our study shows that, under N-rich conditions, one can dope cBN with an excess of C_B substituents relative to C_N, resulting in n-doping of cBN that was observed in experiment. In addition, we find that the dopants prefer to aggregate and form small clusters as opposed to a disordered distribution as seen in random alloys, which is confirmed by the quasi-random structures that we generate. Hence, even though the carbon dopants may not be correlated in the bulk as a whole, they are expected to show local (short length scale) ordering by aggregating into small clusters. These results indicate that the uniform doping by carbon atoms in cBN as observed in experiments by Haque et al.[11] is in fact a uniform distribution of small carbon clusters with an excess of C atoms at the B-sites.

Interestingly, we find that C-doping leads to two types of defects: those that result in easily ionizable states and those that result in polaronic states. We hypothesize that the low temperature conductivity in the transport properties reported by Haque et al.[11] can have contributions from defect-bound small polarons. Further electronic transport measurements at low temperatures coupled with optical spectroscopic techniques should be able to reveal the presence of polarons in experiments.[20] Our work also highlights some of the issues faced with predictable doping of ultrawide band gap semiconductors and can also be extended to materials at lower dimensions.[13] In turn, this work will benefit the research efforts on doping cBN for use in memory devices and optoelectronics capable of functioning under extreme conditions.

https://doi.org/10.1021/acsaelm.2c01743
ACS Appl. Electron. Mater. XXXX, XXX, XXX−XXX

■ ASSOCIATED CONTENT

Supporting Information

The Supporting Information is available free of charge at https://pubs.acs.org/doi/10.1021/acsaelm.2c01743.

Results for the 3 × 3 × 3 supercell, correlation functions for ideal random alloys and special quasi-random structures, phase stability of different dopant clusters, and charge carrier concentrations with respect to $\mathcal{N}_B C_B \mathcal{N}_N C_N$ configurations; electronic density of states and band structures of $\mathcal{N}_B C_B \mathcal{N}_N C_N$ ground state structures and wave functions of defect-polaron states; details of HSE06 calculations and charge transition levels (PDF)

■ AUTHOR INFORMATION

Corresponding Author

Pratibha Dev − *Department of Physics and Astronomy, Howard University, Washington, D.C. 20059, United States;* orcid.org/0000-0002-6884-6737; Email: pratibha.dev@howard.edu

Authors

Sharmila N. Shirodkar − *Department of Physics and Astronomy, Howard University, Washington, D.C. 20059, United States;* orcid.org/0000-0002-9040-5858

Cyrille Armel Sayou Ngomsi − *Department of Physics and Astronomy, Howard University, Washington, D.C. 20059, United States*

Complete contact information is available at: https://pubs.acs.org/10.1021/acsaelm.2c01743

Notes

The authors declare no competing financial interest.

■ ACKNOWLEDGMENTS

We thank Ivan Naumov for helpful discussions and for proofreading the manuscript. This work is supported by National Science Foundation Grant No. ECCS-1831954. This work used the Expanse cluster at SDSC through allocation PHY180014 from the Advanced Cyberinfrastructure Coordination Ecosystem: Services & Support (ACCESS) program, which is supported by National Science Foundation Grants Nos. 2138259, 2138286, 2138307, 2137603, and 2138296, and the Maryland Advanced Research Computing Center.

■ REFERENCES

(1) Miyata, N.; Moriki, K.; Mishima, O.; Fujisawa, M.; Hattori, T. Optical constants of cubic boron nitride. *Phys. Rev. B* **1989**, *40*, 12028−12029.

(2) Tsao, J. Y.; Chowdhury, S.; Hollis, M. A.; Jena, D.; Johnson, N. M.; Jones, K. A.; Kaplar, R. J.; Rajan, S.; Van de Walle, C. G.; Bellotti, E.; Chua, C. L.; Collazo, R.; Coltrin, M. E.; Cooper, J. A.; Evans, K. R.; Graham, S.; Grotjohn, T. A.; Heller, E. R.; Higashiwaki, M.; Islam, M. S.; Juodawlkis, P. W.; Khan, M. A.; Koehler, A. D.; Leach, J. H.; Mishra, U. K.; Nemanich, R. J.; Pilawa-Podgurski, R. C. N.; Shealy, J. B.; Sitar, Z.; Tadjer, M. J.; Witulski, A. F.; Wraback, M.; Simmons, J. A. Ultrawide-Bandgap Semiconductors: Research Opportunities and Challenges. *Advanced Electronic Materials* **2018**, *4*, 1600501.

(3) Chen, K.; Song, B.; Ravichandran, N. K.; Zheng, Q.; Chen, X.; Lee, H.; Sun, H.; Li, S.; Gamage, G. A. G. U.; Tian, F.; Ding, Z.; Song, Q.; Rai, A.; Wu, H.; Koirala, P.; Schmidt, A. J.; Watanabe, K.; Lv, B.; Ren, Z.; Shi, L.; Cahill, D. G.; Taniguchi, T.; Broido, D.; Chen, G. Ultrahigh thermal conductivity in isotope-enriched cubic boron nitride. *Science* **2020**, *367*, 555−559.

(4) Mishima, O.; Tanaka, J.; Yamaoka, S.; Fukunaga, O. High-Temperature Cubic Boron Nitride P-N Junction Diode Made at High Pressure. *Science* **1987**, *238*, 181−183.

(5) Bello, I.; Chong, Y.; Leung, K.; Chan, C.; Ma, K.; Zhang, W.; Lee, S.; Layyous, A. Cubic boron nitride films for industrial applications. *Diamond Relat. Mater.* **2005**, *14*, 1784−1790.

(6) Li, X.; Feng, S.; Liu, X.; Hou, L.; Gao, Y.; Wang, Q.; Liu, N.; Zhang, H.; Chen, Z.; Zheng, J.; Jia, G. Investigation on cubic boron nitride crystals doped with Si by high temperature thermal diffusion. *Appl. Surf. Sci.* **2014**, *308*, 31−37.

(7) Taniguchi, T.; Teraji, T.; Koizumi, S.; Watanabe, K.; Yamaoka, S. Appearance of n-Type Semiconducting Properties of cBN Single Crystals Grown at High Pressure. *Jpn. J. Appl. Phys.* **2002**, *41*, L109.

(8) He, B.; Zhang, W. J.; Zou, Y. S.; Chong, Y. M.; Ye, Q.; Ji, A. L.; Yang, Y.; Bello, I.; Lee, S. T.; Chen, G. H. Electrical properties of Be-implanted polycrystalline cubic boron nitride films. *Appl. Phys. Lett.* **2008**, *92*, 102108.

(9) Kojima, K.; Nose, K.; Kambara, M.; Yoshida, T. Effects of magnesium doping on growth and electric conductivity of nano-crystalline cubic boron nitride thin films. *J. Phys. D: Appl. Phys.* **2009**, *42*, 055304.

(10) Nose, K.; Oba, H.; Yoshida, T. Electric conductivity of boron nitride thin films enhanced by in situ doping of zinc. *Appl. Phys. Lett.* **2006**, *89*, 112124.

(11) Haque, A.; Narayan, J. Tunable n-Type Conductivity and Transport Properties of Cubic Boron Nitride via Carbon Doping. *ACS Applied Electronic Materials* **2021**, *3*, 1359−1367.

(12) Joshi, T.; Kumar, P.; Poudyal, B.; Russell, S. P.; Manchanda, P.; Dev, P. Doping limitations of cubic boron nitride: Effects of unintentional defects on shallow doping. *Phys. Rev. B* **2022**, *105*, 054101.

(13) Weston, L.; Wickramaratne, D.; Van de Walle, C. G. Hole polarons and *p*-type doping in boron nitride polymorphs. *Phys. Rev. B* **2017**, *96*, 100102.

(14) Chen, C.; Avila, J.; Wang, S.; Wang, Y.; Mucha-Kruczyński, M.; Shen, C.; Yang, R.; Nosarzewski, B.; Devereaux, T. P.; Zhang, G.; Asensio, M. C. Emergence of Interfacial Polarons from Electron−Phonon Coupling in Graphene/h-BN van der Waals Heterostructures. *Nano Lett.* **2018**, *18*, 1082−1087.

(15) Austin, I. G.; Clay, B. D.; Turner, C. E. Optical absorption of small polarons in semiconducting NiO and CoO in the near and far infra-red. *Journal of Physics C: Solid State Physics* **1968**, *1*, 1418.

(16) Zunger, A.; Malyi, O. I. Understanding Doping of Quantum Materials. *Chem. Rev.* **2021**, *121*, 3031−3060.

(17) Seager, C. Electronic conduction in Zr-doped TiO2. *Solid State Commun.* **1976**, *20*, 539−542.

(18) Tian, Y.; Li, Y.; He, M.; Putra, I. A.; Peng, H.; Yao, B.; Cheong, S. A.; Wu, T. Bound magnetic polarons and p-d exchange interaction in ferromagnetic insulating Cu-doped ZnO. *Appl. Phys. Lett.* **2011**, *98*, 162503.

(19) Lany, S. Predicting polaronic defect states by means of generalized Koopmans density functional calculations. *physica status solidi (b)* **2011**, *248*, 1052−1060.

(20) Franchini, C.; Reticcioli, M.; Setvin, M.; Diebold, U. Polarons in materials. *Nature Reviews Materials* **2021**, *6*, 560−586.

(21) Wu, G.; Neumeier, J. J. Small polaron transport and pressure dependence of the electrical resistivity of $La_{2-x}Sr_xNiO_4 (0 \leq x \leq 1.2)$. *Phys. Rev. B* **2003**, *67*, 125116.

(22) Giannozzi, P.; Baroni, S.; Bonini, N.; Calandra, M.; Car, R.; Cavazzoni, C.; Ceresoli, D.; Chiarotti, G. L.; Cococcioni, M.; Dabo, I.; Dal Corso, A.; de Gironcoli, S.; Fabris, S.; Fratesi, G.; Gebauer, R.; Gerstmann, U.; Gougoussis, C.; Kokalj, A.; Lazzeri, M.; Martin-Samos, L.; Marzari, N.; Mauri, F.; Mazzarello, R.; Paolini, S.; Pasquarello, A.; Paulatto, L.; Sbraccia, C.; Scandolo, S.; Sclauzero, G.; Seitsonen, A. P.; Smogunov, A.; Umari, P.; Wentzcovitch, R. M. QUANTUM ESPRESSO: a modular and open-source software

project for quantum simulations of materials. *J. Phys.: Condens. Matter* **2009**, *21*, 395502.
(23) Vanderbilt, D. Soft self-consistent pseudopotentials in a generalized eigenvalue formalism. *Phys. Rev. B* **1990**, *41*, 7892−7895.
(24) Perdew, J. P.; Burke, K.; Ernzerhof, M. Generalized gradient approximation made simple. *Physical review letters* **1996**, *77*, 3865.
(25) Grau-Crespo, R.; Hamad, S.; Catlow, C. R. A.; de Leeuw, N. H. Symmetry-adapted configurational modelling of fractional site occupancy in solids. *J. Phys.: Condens. Matter* **2007**, *19*, 256201.
(26) Zunger, A.; Wei, S.-H.; Ferreira, L. G.; Bernard, J. E. Special quasirandom structures. *Phys. Rev. Lett.* **1990**, *65*, 353−356.
(27) Wei, S.-H.; Ferreira, L. G.; Bernard, J. E.; Zunger, A. Electronic properties of random alloys: Special quasirandom structures. *Phys. Rev. B* **1990**, *42*, 9622−9649.
(28) van de Walle, A.; Tiwary, P.; de Jong, M.; Olmsted, D.; Asta, M.; Dick, A.; Shin, D.; Wang, Y.; Chen, L.-Q.; Liu, Z.-K. Efficient stochastic generation of special quasirandom structures. *Calphad* **2013**, *42*, 13−18.
(29) Dev, P.; Xue, Y.; Zhang, P. Defect-Induced Intrinsic Magnetism in Wide-Gap III Nitrides. *Phys. Rev. Lett.* **2008**, *100*, 117204.
(30) Dev, P.; Zhang, P. Unconventional magnetism in semiconductors: Role of localized acceptor states. *Phys. Rev. B* **2010**, *81*, 085207.
(31) Dev, P. Fingerprinting quantum emitters in hexagonal boron nitride using strain. *Phys. Rev. Research* **2020**, *2*, 022050.
(32) Yang, J.-H.; Yakobson, B. I. Unusual Negative Formation Enthalpies and Atomic Ordering in Isovalent Alloys of Transition Metal Dichalcogenide Monolayers. *Chem. Mater.* **2018**, *30*, 1547−1555.
(33) Shirodkar, S. N.; Waghmare, U. V.; Fisher, T. S.; Grau-Crespo, R. Engineering the electronic bandgaps and band edge positions in carbon-substituted 2D boron nitride: a first-principles investigation. *Phys. Chem. Chem. Phys.* **2015**, *17*, 13547−13552.
(34) Bredas, J. L.; Street, G. B. Polarons, bipolarons, and solitons in conducting polymers. *Acc. Chem. Res.* **1985**, *18*, 309−315.
(35) Setvin, M.; Franchini, C.; Hao, X.; Schmid, M.; Janotti, A.; Kaltak, M.; Van de Walle, C. G.; Kresse, G.; Diebold, U. Direct View at Excess Electrons in TiO_2 Rutile and Anatase. *Phys. Rev. Lett.* **2014**, *113*, 086402.
(36) Reticcioli, M.; Setvin, M.; Schmid, M.; Diebold, U.; Franchini, C. Formation and dynamics of small polarons on the rutile $TiO_2(110)$ surface. *Phys. Rev. B* **2018**, *98*, 045306.
(37) Dey, M.; Singh, A.; Singh, A. K. Formation of a Small Electron Polaron in Tantalum Oxynitride: Origin of Low Mobility. *J. Phys. Chem. C* **2021**, *125*, 11548−11554.
(38) Krukau, A. V.; Vydrov, O. A.; Izmaylov, A. F.; Scuseria, G. E. Influence of the exchange screening parameter on the performance of screened hybrid functionals. *J. Chem. Phys.* **2006**, *125*, 224106.
(39) Coutinho, J. Theory of the Thermal Stability of Silicon Vacancies and Interstitials in 4H−SiC. *Crystals* **2021**, *11*, 167.
(40) Guster, B.; Melo, P.; Martin, B. A. A.; Brousseau-Couture, V.; de Abreu, J. C.; Miglio, A.; Giantomassi, M.; Côté, M.; Frost, J. M.; Verstraete, M. J.; Gonze, X. Fröhlich polaron effective mass and localization length in cubic materials: Degenerate and anisotropic electronic bands. *Phys. Rev. B* **2021**, *104*, 235123.

https://doi.org/10.1021/acsaelm.2c01743
ACS Appl. Electron. Mater. XXXX, XXX, XXX−XXX